IEEE Access
Multidisciplinary ⋮ Rapid Review ⋮ Open Access Journal

Received 29 December 2023, accepted 22 January 2024, date of publication 30 January 2024, date of current version 12 February 2024.

Digital Object Identifier 10.1109/ACCESS.2024.3360223

RESEARCH ARTICLE

Improved Segmentation Model for Melanoma Lesion Detection Using Normalized Cross-Correlation-Based *k*-Means Clustering

MUHAMMAD IMRAN FAIZI AND SYED MUHAMMAD ADNAN
Department of Computer Sciences, University of Engineering and Technology Taxila, Taxila 47080, Pakistan
Corresponding author: Muhammad Imran Faizi (imran.faizi@uettaxila.edu.pk)

ABSTRACT The most unexpected and fatal kind of cancer, melanoma, has been on the rise in its spread to different parts of the body. Early detection can significantly reduce its fatality rate. The primary stages of melanoma for its identification by the unaided eye are a difficult task that demands extensive training and understanding. Due to a lack of qualified dermatologists, a computerized and automated method is required to correctly detect melanoma. This study achieved this feat through a proposed system that can effectively detect and classify melanoma as benign or malignant. The process begins with image template matching by using normalized cross-correlation technique induction to mark the infected area of skin lesion as the region of interest (ROI) from ISIC datasets 2017, 2019, and 2020 dermoscopic images. Our novel model dynamically calculated number of clusters is assigned to the *k*-means clustering algorithm, and ROI is extracted. Histogram equalization is applied to the output image for contrast enhancement. Hu Moment method is implemented for shape classification and part recognition from the segmented image. GLCM-based Haralick feature extractor is used in the proposed system to extract textural features generating the feature vector from the segmented skin lesion. It leads the classifier to identify skin lesions as cancerous or non-cancerous. Random Forest, Decision Tree, Support Vector Machine (SVM), Gaussian Naïve Bayes, Logistic Regression, and K-nearest neighbor (KNN) Classifiers are used for classification. The KNN, SVM, and Random Forest was successful in attaining the highest accuracy of 99.29%, 99.38%, and 99.46% on the given dermoscopic images datasets ISIC-2019, ISIC-2020 and ISIC-2017 respectively. The proposed method, the normalized cross correlation-based k-means clustering model, was found to be more robust and accurate than existing methods and incorporates much more feature information from the images.

INDEX TERMS Melanoma, image processing, computer vision, classification, template matching.

I. INTRODUCTION

This tumor can be benign or malignant. Benign (noncancerous) tumors are slow in growth and do not spread. Malignant (cancerous) tumors can grow rapidly, attack and destroy adjacent normal tissues, and spread throughout the body. Therefore, recognized as the most serious type of skin cancer; deaths are reported mostly due to this disease. Qualified and expert dermatologists can inspect the infected skin lesion through Dermoscopy, and more clinical examinations are applied if the case is more sensitive. A 95% chance exists to cure skin cancer patients if the disease is at the initial stage [1]. Prominent outcomes are achieved in the recognition of diseased images by computer vision and machine learning using a large number of image sets [2]. Solutions based on artificial intelligence (AI) are actively considered by researchers to diagnose melanoma automatically using infected skin lesion images by applying both traditional as well as deep learning methodologies [3], [4], [5], [6], [7], [8]. Melanoma and non-melanoma imbalanced datasets and less collection of images lead researchers to tackle these challenges more deeply. ISIC published a freely available dataset in 2019, having 25331 dermoscopic images with eight different types of melanoma diseases [2]. It is mandatory to detect

The associate editor coordinating the review of this manuscript and approving it for publication was Vishal Srivastava.

and localize infected skin lesions in the image to estimate the number of distinct features that exist for accurate diagnosis of cancer. Boundaries of the skin lesion are more difficult to determine accurately, if so, it ensures higher computation accuracy of maximum diameter, boundary irregularity, and color attributes [9]. At first, skin lesion boundaries are marked to detect cancer by applying image segmentation strategies. Then the texture-color image was discriminated against by color and texture distributions. The segmentation procedure enabled the early detection of skin cancer [10], [11], [12], [13], [14], [15], [16].

Segmentation is the process of removing extraneous information from the provided image. Manual border detection is used in existing algorithms for segmentation. Thresholding algorithms, region growing and merging, and dynamic programming are the most used segmentation techniques [17], [18], [68]. In malignant melanoma recognition frameworks preoccupied with the conventional clinical calculation of the ABCD rule of dermoscopy, feature extraction algorithms are employed to describe the lesion. The primary characteristics of a wound are identified during this phase, including its dimension, spatiality, and border irregularity. Between feature extraction and classification comes a phase called feature selection [19], [20]. In this procedure, the initial feature vector acquired in the feature extraction stage is less important, and weak features are omitted. The two most popular feature selection techniques utilized in most common computer-based skin cancer recognition systems are the stepwise progressive approach and cross-correlation feature selection [21], [22]. Classification is the final step of identification in which the selected features are used to determine whether the lesion is cancerous. Linear Regression, Random Forest, Decision Tree, SVM, ANN, and KNN are common classifiers.

The proposed system, a normalized cross-correlation-based k-means clustering model, employs the operations named image refinement, detection of ROIs, image localization, features extraction and selection, and classification. The evaluation parameters accuracy, sensitivity, specificity, and F1-score are used to evaluate the performance of the proposed work. Our contributions are as follows:

1. A local template mask is used as a source in the template matching algorithm using a normalized cross-correlation technique to find the exact locations of the target contents (malignant melanoma) in the main image. These locations result in acquiring the number of clusters which is later referred to as the number of k dynamically calculated clusters in high-performance classical algorithm k-means clustering algorithm for improved segmentation

2. Since K-means highly depend on the fixed number of clusters k and randomly initialized centroids it may lead to poor quality of clustering [26]. Since, in our case, the number of skin lesion areas varies. Therefore, we have passed a dynamic number of clusters k, obtained from Normalized Cross Correlation. As far as initial centroids are concerned, we have calculated the centers of rectangular regions obtained through Normalized cross-correlation. We proposed a novel improved segmentation technique using normalized cross-correlation-based k-means clustering.

3. We have combined the features extracted by the Haralick texture and Hu-Moment shape features. This outperformed all state-of-the-art algorithms and achieved higher accuracy with low computational cost.

II. LITERATURE REVIEW

Researchers [18] accurately identify the damaged regions using RetinaNet, with bounding boxes around several different regions. In addition, a conditional random field (CRF) is used to locate segmented melanoma lesions. The author carried out three steps: melanoma segmentation, melanoma localization, and image pre-processing using the benchmark datasets, Pedro Hispano (PH2) and ISIC 2018. Experimental results demonstrated high performance. Pixel-level sensitivity is 93.20%, pixel-level specificity is 97.70%, pixel-level accuracy is 94.20%, dice coefficient is 93.10%, and Jaccard index is 91.87% for the ISIC 2018 challenge data.

In this study [20], for the detection and categorization of skin lesions, a 38-layer deep learning simulation was developed. The HAM10000 dataset and the ISIC2019 dataset were the two datasets utilized for training and testing. The model performed better than expected on both datasets, proving that it is independent of the dataset, according to experimental results. On the HAM10000 dataset, 94.45% of the top three accuracy results from validation were attained, and on the ISIC2019 dataset, 93.06%.

The author [66] used U-net and LinkNet models with additive properties of transfer learning and fine-tuning methods to segment the melanoma from the infected lesion. The author of this research article also evaluated the learning capabilities of the proposed model, and how accurately segments the malignant region from the normal skin. The model was tested on publicly available datasets ISIC 2018, DermIS, and HP2 and achieved Dice 89.3 on the ISIC 2018 dataset, Dice 87.9% on DermIS, and PH2 an average Dice was 92.3%.

In this research [67], the researcher proposed an explainable CNN-based stacked ensemble framework for early-stage melanoma detection. In his proposed model, multiple CNN sub-models with transfer learning techniques assembled the same classification task. They examined their framework by using an open-access dataset containing benign and malignant melanoma images. The developed method visualized melanoma images by producing heatmaps to explain the shapes of the disease most indicatively which creates more ease of identifying the malignant or benign to the dermatologist. The ensemble model showed effective results with an accuracy of 95.76%, a sensitivity of 96.67%, and an AUC of 95.7%.

According to the author [23], dermoscopic images should be segmented using the Canny Detector to identify irregular lesion borders. Among the ABCD rules, rule B is mostly utilized to classify cancer as benign or malignant. With accuracy, sensitivity, specificity, and F-scores of 93.6%, 100%,

92.5%, and 96.1%, respectively, the method produces excellent results.

First [24], the author presented an improved version of Otsu's approach for skin lesion segmentation along with pre-processing and post-processing stages. The decision tree algorithm, which acts as a classifier, is then trained and tested using a vector of three metrics (SIFT-based similarity, Projection profiles, and Skewness). The CIELab color space and Minkowski distance are used to identify the lesion's colors for ''color variegation.'' The ''diameter'' of the skin lesion is measured as the maximum Ferret's diameter (caliper diameter), which is the separation between two parallel tangents along the object's contour. When turning the resulting diameter pixels into a spatially calibrated image for 256×256 images with 29.7 pixels/mm (image in unit mm). The accuracy achieved by the researchers was 80.00%.

In this study [25], the researcher used one clinical information module, hand-crafted biologically inspired modules, and knowledge transfer over the ResNet-50 network. They achieved an AUC of 87.00% for the ResNet-50 deep learning-based classifier and an AUC of 90.00% for the conventional image processing-based classifier, yielding a classification accuracy of 94.00%, 87.00%, and 90.00%, respectively.

According to the author [26], a total of 39 segmentation algorithms are defined and used in comparison in the suggested system. Seven categories are used to group these techniques. Threshold, Clustering, Fuzzy Methods, Quantization, Active Contours, Merging Threshold, and Pattern Clustering are a few examples. The two approaches that perform the best are LBP and k-means clustering. They provided more accurate results than other methods.

The researcher [27], used HOG and Automated Features Fusion [80:20 training and test division], a state-of-the-art technique that uses two manually created descriptors and one automated feature learning feature extraction technique explored for classification performance, and they were successful in achieving Specificity: 97.00% and Sensitivity: 62.00%.

In this research [28], the author employed the datasets PH2, ISBI2016, and ISIC2017. Fusion-based Contrast Stretching, FRG-based Segmentation, Graphcut-based Segmentation, Multilevel Feature Extraction, and HOG, SURF Classification are the three processes that make up this system. With accuracy ratings of 95.86%, 94.79%, and 94.92% on PH2, ISBI2016, and ISIC2017, respectively, the segmentation performance is assessed. The accuracy of the classification performance is examined using the PH2 and ISBI2016 datasets, with 98.20% and 95.42% accuracy, respectively.

The authors of this study [29] proposed an autonomous ''melanoma recognition system,'' which relied on deep learning techniques in conjunction with ''RSurf'' features and ''local binary patterns'' LBP. They combined SVM and CNN. They made use of the ISIC dataset. Their classification accuracy was 82.6%, their sensitivity was 53.3%, and their specificity was 89.8%.

In this research [21], the author processed and segmented the database of the dermoscopic images using thresholds and histogram equalization. Four steps of statistical feature extraction utilizing the Grey Level Co-occurrence Matrix are used (11 features). SVM is used to classify the remaining few features after PCA (4 features) selection. The accuracy of the SVM classifier, which uses 11 features in total, is 92.10%, and the accuracy of the PCA, which uses 5 features, is also 92.10%.

The proposed study [30] employs traditional machine learning techniques like deep residual networks and fully convolutional neural networks together with more contemporary ones like hand-coded feature extractors, sparse coding techniques, and SVMs. Three feature extraction techniques include the color histogram, edge histogram, and multi-scale color Local Binary Patterns (LBP). They were 93.1% accurate. The first task's accuracy was 94.90% and specificity was 92.80%; the second task's accuracy was 73.90% and sensitivity and specificity were both 74.30%. In contrast, previous pre-made models produce an accuracy of 91.20%.

According to the given work [31], 84 directional filters to preprocess the skin images. SVM is used for classification after OTSU threshold-holding lesion segmentation. They attained a 96.30% accuracy rate.

This approach used two separate approaches, the first global technique employs feature extraction using a gradient histogram, segmentation with wavelets, Laplacian pyramids, or linear filters, followed by a binary classifier for classification [32]. Bag of Features (BoF) classifiers are used for image processing tasks in the second approach of local features. Accuracy increased by 87.00%.

The most recent method is presented in this publication [33]; hair removal was carried out during image preparation. Utilizing a color-based OTSU threshold, image segmentation is accomplished. Shape, color, and texture features are extracted during feature extraction. Finally, classification using decision trees achieved an accuracy of 85.00%.

In this research [13], the author suggested combining type-2 fuzzy logic and the thresholding approach. They first convert the input dermoscopic image to grayscale before computing its histogram, which is used to determine the ideal threshold value. The most popular Otsu method and adaptive thresholding are contrasted with this approach. Compared to the actual border irregularity, Otsu's and adaptive thresholding both artificially increase the irregularity of borders. Inconsistency is also an indication of melanoma. Both techniques are therefore more accurate.

The researcher [34] used a dataset of 588 images in this proposed work, comprising more than 200 melanoma cases, an ANN classifier was trained in this instance. They produce 48 traits that can be divided into four groups: shape, color, texture, and islands of color. The 13 features that remained after the feature selection procedure were split into two groups: form and color. They delivered results with a 94.00% accuracy rate.

In this research [35], the author utilized solely form and color features, they created a Nearest neighbor-based algorithm. Their system's goal is to divide these traits into three categories—benign, dysplastic, and malignant—based on how they were found and extracted. 5393 daily clinical lesion images are used as a dataset for the evaluation portion. A feature selection procedure is used to acquire, extract, and then condense a total of 122 features to just 21. On the used dataset, the overall experimental findings show 93.00% specificity and 87.00% sensitivity.

The author [63] says that skin cells develop abnormally, which leads to skin cancer. It is critical to recognize this alteration in skin cells as soon as possible because failure to do so could be fatal to humans. More dangerous skin cancer is called malignant melanoma, or melanoma. Melanoma detection that is both accurate and automatic is very important because it aids in the diagnosis process. To improve segmentation outcomes, the suggested model enhances the texture region using the Histogram (HE) and Adaptive Gamma Correction with Weighting Distribution (AGCWD) techniques. Moreover, the suggested model combines DeepLabV3+ with several base networks, including ResNet 18, ResNet 50, and MobileNetV2, to automatically detect skin lesions. A range of images from the ISIC 2016, ISIC 2017, and ISIC 2018 datasets are used to test the suggested model. The suggested model is assessed by contrasting it with the current methods.

In this paper [64], the author identified that the quality of the biomedical image dataset significantly affects the model's performance. It has been observed that a few factors, including illumination, camera, and angle, cause insufficient contrast in images, which leads to the generation of insufficient image features. Consequently, improving the image is an essential pre-processing step that can significantly boost CNN models' performance. For the MNIST medical dataset, this paper suggests integrating the CNN model with illumination normalization techniques to improve classification accuracy. Tantrigg and isotropic illumination enhancement techniques have been combined with mobileNetV2 and squeezeNet conventional networks in this work. With Tantrigg combined with conventional CNN models, the best result of 99.13% is achieved out of all the approaches. Likewise, the integration of Isotropic with conventional CNN models yields the best result, which stands at 98.20%. Numerous tests and findings show that the recommended approach is effective in handling unevenly lit images and produces higher classification accuracy.

The author's [65] technique described in this research uses fast fuzzy c-means (FCM) based on MMLVR-WT to extract lesions from dermoscopic images in an unsupervised manner. The suggested technique creates super-pixels from images using MMLVR-WT, then computes the super-pixel images' histogram to provide fast fuzzy c-means (FCM). The approach is evaluated by taking into account a large range of images on several publicly accessible datasets, including ISIC 2016, ISIC 2017, and ISIC 2018. The suggested method may accurately extract the lesions despite being an unsupervised approach. It has a sensitivity of 95.76%, specificity of 98.96%, Jaccard index of 89.1%, dice coefficient of 93.56%, and total accuracy of 96.7%.

In this paper [66], the author presented a novel unsupervised skin melanoma extraction and analysis method. The suggested technique starts by removing hairs from dermoscopic images before extracting skin lesions using a straightforward thresholding-based method. Additionally, a color grading system is used to analyze the excised skin lesions to validate the presence of melanocytic cells. The suggested technique is quantitatively contrasted with the most advanced skin lesion extraction techniques currently in use. The proposed approach is superior, as demonstrated by the experimental findings, which show an average accuracy of 93% and 96% for the ISIC 2016 and ISIC 2018 datasets, respectively.

By merging the DeepLabV3 + with several base networks, including ResNet-50, ResNet-18, and MobileNetV2, [67] the research proposes a unique convolutional neural network (CNN)-based deep learning technique. By not requiring images to be preprocessed, the suggested model reduces the algorithm's complexity. To train and test the suggested model, images from the ISIC 2016, 2017, and 2018 datasets are taken into account. Several performance measurement criteria, including accuracy, the Jaccard Index (JI), and the Dice Coefficient (DC), are computed for the various datasets to validate the proposed model. The suggested model yields a DC of 90%, JI of 89%, and Accuracy of 93%. This demonstrates how the suggested model is better than the most advanced techniques.

A clustering-based technique for melanocytic lesion extraction is developed in this research [68]. The original dermoscopic images are processed by the algorithm to extract lesions. The dermoscopic images are first pre-processed to eliminate artifacts such as ruler markings, gels, hairs, and so on. In addition, mean shift clustering is used to separate lesion features from those of healthy areas. In addition, morphological operations are used in the post-processing of the feature image to remove lesions from dermoscopic images. The suggested approach is evaluated using publicly accessible datasets, including PH2, ISIC 2016, ISIC 2017, and ISIC 2018, both numerically and qualitatively. The average accuracy across all datasets is 93.76%, which may be compared to other methods that have been created thus far.

III. PROPOSED METHODOLOGY

In this proposed work, we introduced a novel method for locating a portion of a skin lesion from input images utilizing two templates, one for malignant and the other for benign. We proposed a novel segmentation technique, a normalized cross correlation-based k-means clustering model, to improve the segmentation process. Conventionally the k-means clustering technique for segmentation requires the number of clusters as input from the user. It may work well for a single image that is a subjective matter. In the case of large datasets where we deal with a huge number of images, it's

not appropriate to manually define the number of clusters k as the input parameter. And if we fix this number for all images, then it can severely affect the results. In our proposed work we cope with it by introducing the dynamic clustering method to improve the segmentation model using normalized cross-correlation-based k-means clustering. Here we used a template matching technique where a template of a local mask goes on the process of normalized cross-correlation and finds its matching signals in an image. These spikes in the signal are counted as the number of ks and referred to as dynamically found clusters in the current image. This number is then forwarded to the k-means clustering algorithm for further clustering-based segmentation. The output of this segmentation is then processed to extract features using a GLCM-based Haralick feature extractor. Later on, the feature selection by PCA is applied and the final vector is passed to the well-known classifiers.

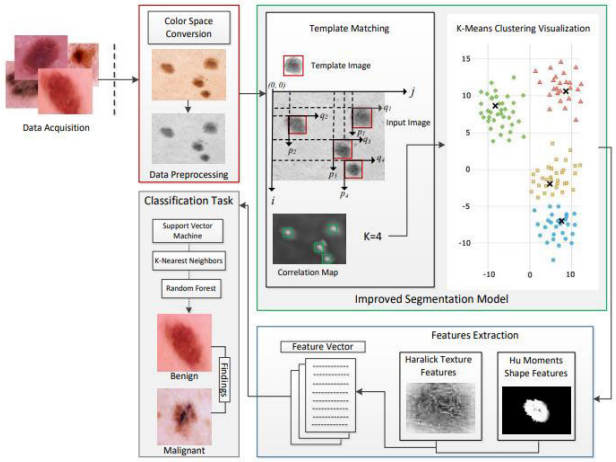

FIGURE 1. Proposed methodology block diagram with improved segmentation.

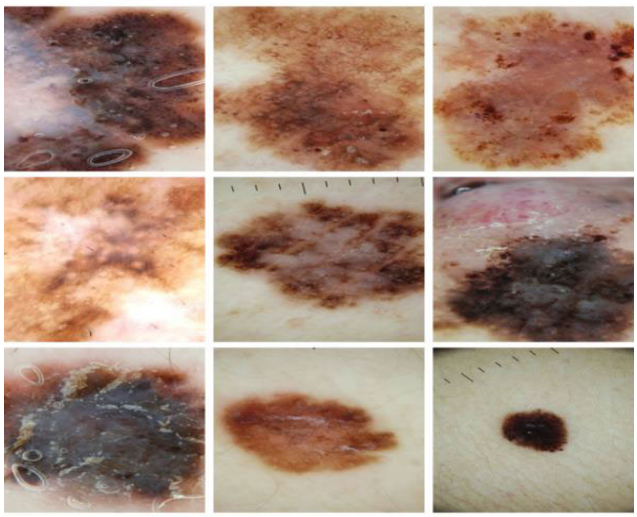

FIGURE 2. Malignant dataset images.

Following is the proposed algorithm and process details:

Algorithm 1 Proposed Algorithm

```
Begin
    Timg = ReadImage(TempPath)
    XFeatures[ ] = 0
    YLabel[ ]
    ForEach folder in DataSet.Folder
        ForEach file in folder
                Img = ReadImage(file)
            MatchTemplate(img,timg,method =
            Normalized_Correlation)
        End For
        k = 0
        ForEach matchedArea in img
            k = k+1
        End For
    End For
    Kmeans = KMeans(noofclusters = k)
            ResImg = kmeans.predict(img)
    Humu = Humument(ResImg)
    Har = Haralick(ResImg)
    FeatureVactor = concatFeatures(Humu,har)
    Ylabel.Append(folder.Name)
    XFeature.add(FeatureVactor)
    Model Training
end
```

A. DATASET AND PRE-PROCESSING

In this research, the publicly available dataset of skin lesions was acquired from ISIC (International Skin Imaging Collaboration) archives in 2017, 2019, and 2020. We divide the dataset that is containing ISIC 2017, 2690 images (divided into 1593 benign, and 1167 malignant), ISIC 2019, 990 images (divided into 572 benign and 418 malignant)

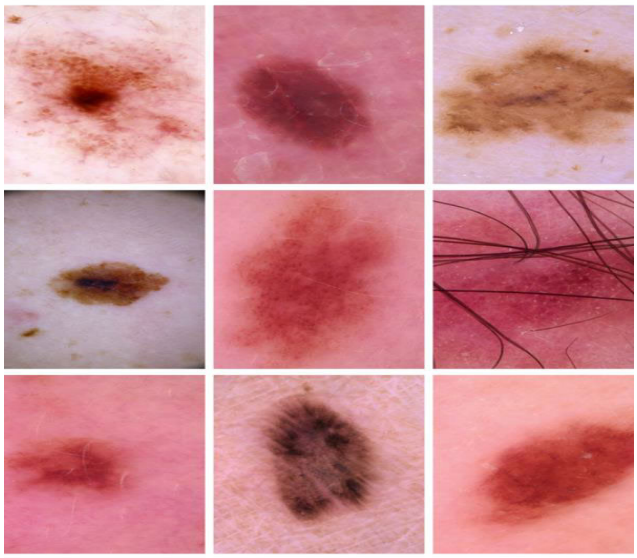

FIGURE 3. Benign dataset images.

and ISIC 2020, 2760 images (divided into 1537 benign and 1223 malignant) moles. The dataset is divided into training and testing, parted that into 70% and 30% respectively [55]. Acquired dataset skin lesion images are found in RGB form. To reduce the computation requirements and enhance image visualization, the dataset is transformed into grayscale [15], [16].

B. TEMPLATE MATCHING

One image is chosen from the dataset and manually crafted an infected region of size 100×100 having black dots, brown dots, spread shape of melanoma, and pigment network is present, as a template to match one by one and marked the segment as a rectangle around the region of interest (ROI). Binary image refers to the process of converting a color image to a white and black image and gray levels. This approach is entirely dependent on various color transformations. It evaluates the grey scale values and creates the grey image based on the image's R, G, and B values. Using the example graphic, a small section of the input image may be used as the template image, which is then used to locate the template within the search image. Use template matching techniques [36] such as the sum of squared differences, cross-correlation, and normalized cross-correlation [37], [38], [39], [40]. After that, compare the images to the original images.

By looking for a match between an object template u(m,n) and the image v, one can determine whether or not an image contains a recognized item (m,n). One method of achieving this is by calculating the cross-correlation between the template and the image [41]. For a displacement (p,q), the cross-correlation is given below equation:

$$C_{vu}(p,q) = \sum_{m}\sum_{n} v(m,n)\, u(m-p, n-q) \qquad (1)$$

C. IMPROVED SEGMENTATION MODEL FOR K-MEANS CLUSTERING

The segmentation process is a crucial step in image processing and pattern recognition. The k-means algorithm is one of the most widely used techniques for image segmentation due to its simplicity and efficiency [62]. It is a clustering algorithm that partitions the input data into K clusters based on their similarity. The algorithm works by initializing K centroids and then repeatedly reassigning each pixel to the cluster with the closest centroid until convergence. The result is a segmented image where each pixel is assigned to a cluster and the pixels within each cluster are similar to each other [63]. This algorithm can be used to segment images into foreground and background, to detect objects, or to separate different regions of interest. The choice of the number of clusters, k, and the initialization of the centroids are crucial factors that can affect the performance of the k-means algorithm [18], [26].

FIGURE 4. Malignant melanoma template input image.

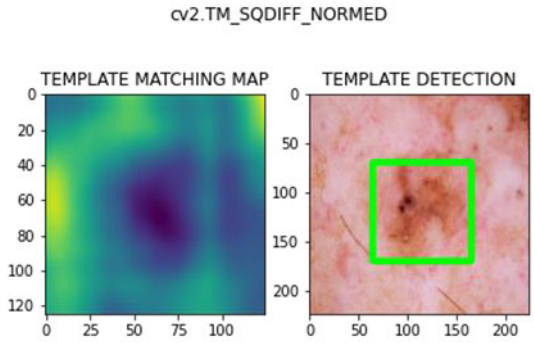

FIGURE 5. Template detected in the image.

By tradition, the k-means clustering technique for segmentation requires the number of clusters as input from the user. It may work well for a single image that is a subjective matter. In the case of large datasets where we deal with a huge number of images, it's not appropriate to manually define the number of clusters k as the input parameter. If we fix this number for all images, then it can severely affect the results. In our proposed work we deal with it by introducing the dynamic clustering method. Here we used a template matching technique where a template of a local mask goes on the process of normalized cross-correlation and finds its matching signals in an image.

$$\mu_{ij}(x,y) = \frac{\sigma_{pip_j}(x,y)}{\sigma_{pi}(x,y)\,\sigma_{pj}} \qquad (2)$$

These spikes in the signal are counted as the number of ks and referred to as dynamically found clusters in the current image. This number is then forwarded to the k-means clustering algorithm for its further clustering-based segmentation. The output of this segmentation is then processed to extract features. Segmentation results are shown here.

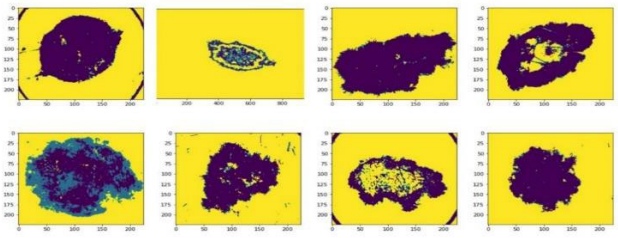

FIGURE 6. Malignant results after k-means clustering.

D. SIGNAL SPIKES BY NCC

k-means algorithm is used for finding ROI. In our case, the region of interest is those areas where there are skin

lesions. NCC is roughly finding those areas and the number of clusters. And then by using k-means exact segments of skin lesions are found. Moreover, the performance of k-means depends on the number of clusters and the centers which are randomly selected initially. We have improved k-means, by passing the centroids array by finding the centers of all rectangular regions given by NCC. Spikes in the signal are counted as the number of ks and referred to as dynamically found clusters in the current image. The spike is shown in Figure 7(a).

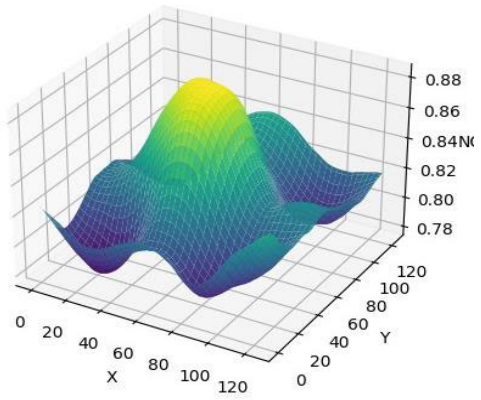

FIGURE 7. Spike shown by NCC.

E. FEATURE EXTRACTION

Textual and shape feature extractions are important steps in image processing and computer vision, as they allow us to extract important information from an image. The Haralick algorithm is a texture feature extraction method [49] that is widely used in the field of image analysis. It is based on the concept of gray-level co-occurrence matrices (GLCMs) [50], which represent the statistical relationship between pairs of pixels in an image. The Haralick algorithm calculates various statistical measures, such as energy, entropy, correlation, and homogeneity [48], from the GLCMs to represent the texture of an image. These features are then used to differentiate between different textures in the image and to classify the image based on its texture. The Haralick algorithm [47] is simple, efficient, and effective for texture feature extraction. [19], [20]. The Hu-Moments algorithm is a popular method for shape feature extraction, which is based on the theory of image moments. Image moments are statistical descriptions of the distribution of pixel intensities in an image, and they can be used to represent the shape of objects. The Hu-Moments algorithm calculates seven invariant moments that are invariant to translation, rotation, and scaling. These moments can be used to represent the shape of an object and to distinguish between different shapes. The Hu-Moments algorithm is simple, fast, and effective for shape feature extraction for object recognition, image matching, and image retrieval [45], [46].

F. CLASSIFICATION

Image classification is the process of assigning a label to an image based on its content. Several algorithms can be used for image classification, and we applied and compared the results of the Random Forest, Decision Trees, Support Vector Machines (SVM), Gaussian Naive Bayes, Logistic Regression, and K-Nearest Neighbor (K-NN).

Random Forest is an ensemble learning algorithm that combines multiple decision trees to improve the accuracy of predictions. It is a flexible and powerful method that can handle complex data and non-linear relationships [56]. Decision Trees are a simple and intuitive algorithm for image classification. They work by recursively partitioning the data into smaller regions based on the features of the data, and making predictions based on the majority class of each region [57]. Support Vector Machines is a powerful algorithm for image classification that works by finding a hyperplane that separates the data into different classes. It is often used for high-dimensional data and can handle non-linear relationships [58]. Gaussian Naive Bayes is a probabilistic algorithm for image classification that is based on Bayes' theorem. It is a fast and simple algorithm that makes predictions based on the probability of each class given the input data [59]. Logistic Regression is a linear classification algorithm that models the relationship between the input data and the class labels. It is a simple and fast algorithm that is often used for binary classification problems [60]. K-Nearest Neighbor (K-NN) is a simple and intuitive algorithm for image classification. It works by finding the K closest training samples to the input data and making predictions based on the majority class of these samples [61].

G. EVALUATION PARAMETERS

The following performance evaluation measures, which are defined as follows, are used to conduct the quantitative analysis of the method that is being presented [23]:

$$\text{Sensitivity} = \frac{\text{No. of truely detected malignant images}}{\textit{Total No.of malignant images}}$$

$$\text{Specificity} = \frac{\text{No. of truely detected Benign images}}{\textit{Total No.of benign images}}$$

$$\text{Accuracy} = \frac{\text{No. of truely detected malignant} + \text{benign images}}{\textit{Total No.of malignant} + \textit{benign images}}$$

$$\text{F1 Score} = 2\text{x}\frac{\textit{sensitivity (recall) x specificity(precision)}}{\textit{sensitivity (recall)} + \textit{specificity(precision)}}$$

IV. RESULTS AND DISCUSSION

In this study, we introduced a novel approach that makes use of the image template matching method to recognize

and segment skin lesions from input images. First, the template image is crafted from one of the given ISIC dataset images that contain maximum malignant melanoma features at an early stage. The dataset is divided into 70% training images and 30% test images. The template image is resized to 100×100 and all dataset images are converted from RGB to Grayscale for standard evaluation. Then template matching is applied to mark the spikes and count the infected skin lesion segment. To generate the best result, we applied the k-means clustering by providing the number of clusters (k) dynamically using normalized cross-correlation. Textural and shape Features are extracted by using the Haralick Feature extractor and Hu-Moment respectively. Then, concatenate these features to form a reduced feature vector by using the Principal Component Analysis (PCA) Feature selector. This feature vector is then passed to the classifier to identify malignant or benign moles. We used Random Forest, Decision Tree, SVM, Gaussian Nave Bayes, Logistic Regression, and KNN Classifiers and generate results. The superior performance and efficiency of our novel approach have generated state-of-the-art results. The results produced by the classifiers are as follows:

A. CLASSIFICATION RESULTS

The proposed system has been developed using Python and the Co-Lab platform is used for the compilation and evaluation of the ISIC 2017 dataset of 2760 images, the ISIC 2019 dataset of 990 images, and the ISIC 2020 dataset containing 2760 images. Random Forest, Decision trees, support vector machine (SVM), Gaussian Naïve Bayes, Logistic Regression, and K-nearest neighbor (K-NN) with different kernels are applied to the feature vector. Results are achieved and presented in the form of accuracy for each classifier in the following Table:

TABLE 1. Performance comparison of different machine learning classifiers.

Deep Learning Models	Year	Dataset	Accuracy %
eVida Model 6 [41]	2021	ISIC 2017 challenge	90.4%
Interpretable deep learning and ensemble stacking of ML models[42]	2022	A small dataset of ISIC 2018	92%
MSLANet[43]	2022	ISIC 2017	93.7%
	2022	ISIC2020	92.4%
EfficientNet-B6 (lr 0.00001, Adam)[44]	2023	ISIC 2019	94.86%
	2023	2020	77.65%
spiking VGG-13 model[45]	2023	ISIC 2019	89.57%
Our Proposed Model		ISIC 2017	**99.46%**
		ISIC 2019	**99.29%**
		ISIC 2020	**99.38%**

TABLE 2. Performance comparative study with different deep learning models.

Dataset	ISIC-2017	ISIC-2019	ISIC-2020
Classifier		**Accuracy %**	
Logistic Regression	98.37	98.79	99.02
Gaussian Naïve Bayes	91.09	98.08	91.23
Decision Tree Classifier	99.17	98.48	98.84
Support Vector Machine	74.15	98.48	**99.38**
Random Forest Classifier	**99.46**	98.89	99.09
k-Nearest Nabour Classifier	99.31	**99.29**	98.99

B. K-NEAREST NEIGHBORS CLASSIFIER (K-NN)

Evelyn Fix and Joseph Hodges developed the k-NN [51] in 1951, and Thomas Cover later made improvements to it. It uses supervised learning in a non-parametric manner. On our dataset's benign and malignant image data, the k-NN is applied. The closest k training samples from a data collection make up the input. Class membership is the outcome of the k-NN classification process. The neighbors of an item decide what class to assign it based on a majority vote among its k nearest neighbors (k is a positive integer, typically small). The object is simply assigned to the class of its one nearest neighbor if $k = 1$. Using this classifier, we reached the best accuracy of 99.29% on the ISIC-2019 dataset. Additionally, we looked at precision, recall, and F1-score. The system outperformed the state-of-the-art algorithms using image matching and was able to distinguish between benign and malignant melanoma with greater accuracy.

TABLE 3. Performance of k-NN classifier.

	Precision %	Recall %	F1-Score %	Support
Benign	**99.65**	**99.13**	**99.39**	**572**
Malignant	**98.81**	**99.52**	**99.17**	**418**
Macro Avg	**99.23**	**99.32**	**99.28**	**990**

TABLE 4. Actual and predicted images by k-NN classifier.

N=990	Predicted: Benign	Predicted: Malignant	
Actual Benign	TN=567	FP=5	572
Actual Malignant	FN=2	TP=416	418
	569	421	

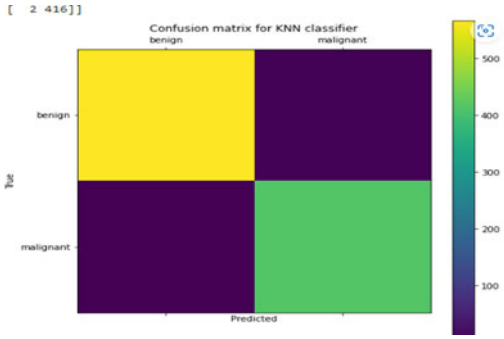

FIGURE 8. Confusion matrix using k-NN classifier.

C. LOGISTIC REGRESSION CLASSIFIER

A dichotomous dependent variable, such as D, and several Xs can be explained using a mathematical modeling technique called logistic regression. This classifier helped us reach an accuracy of 98.08%. Additionally, we investigated F1-score, recall, and precision. The overall classifier results are listed below:

TABLE 5. Performance of logistic regression classifier.

	Precision %	Recall %	F1-Score %	Support
Benign	**99.30**	98.60	98.95	572
Malignant	98.10	**99.04**	98.57	418
Macro Avg	98.70	**98.82**	98.76	990

TABLE 6. Actual and predicted images by LR classifier.

N=990	Predicted: Benign	Predicted: Malignant	
Actual Benign	TN=564	FP=8	572
Actual Malignant	FN=4	TP=414	418
	568	422	

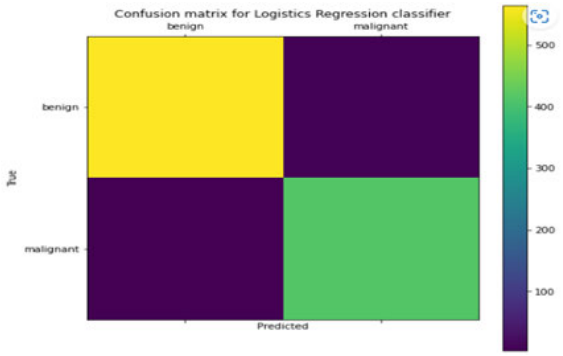

FIGURE 9. Confusion matrix using LR Classifier.

D. NAIVE BAYES CLASSIFIER

Bayesian classifiers are a type of statistical classifier. They can predict things like the likelihood that a given sample will belong to a particular class and other probabilities of class membership. A Bayesian classifier is built on the Bayes theorem. Naive Bayesian classifiers make the premise that the effects of one attribute's value on a given class are independent of the effects of the other attributes' values. This premise is known as ''class conditional independence.'' In this respect, it is considered ''naive'' because it attempts to simplify the computation at hand. With the aid of this classifier, we achieved an accuracy of 98.08%. We also considered F1-score, recall, and precision. Below are the overall classifier results:

TABLE 7. Performance of naive bayes classifier.

	Precision %	Recall %	F1-Score %	Support
Benign	98.95	98.13	**99.04**	572
Malignant	**98.80**	98.56	98.68	418
Macro Avg	**98.88**	98.85	98.86	990

TABLE 8. Actual and predicted images by NB classifier.

N=990	Predicted: Benign	Predicted: Malignant	
Actual Benign	TN=567	FP=6	572
Actual Malignant	FN=5	TP=412	418
	572	418	

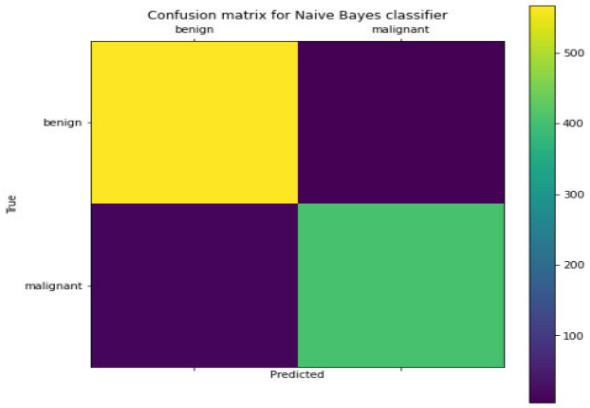

FIGURE 10. Confusion matrix using NB Classifier.

E. SVM CLASSIFIER

To train and test our Support Vector Machine (SVM) [52] classifier, we employ labeled feature sets from the image dataset. Given the feature set that was recovered (from

benign and melanoma photos), the SVM classifier created a maximum-margin hyperplane that effectively separated the two classes of data. The distance between the hyperplane and the closest training point is referred to as the margin. Support vectors are hyperplane vectors. This classifier helped us to reach the highest accuracy of 99.38% on the ISIC 2020 dataset. We also investigated F1-score, recall, and precision. The findings of the classifier are as follows:

TABLE 9. Performance of SVM classifier.

	Precision %	Recall %	F1-Score %	Support
Benign	97.59	**99.13**	98.35	572
Malignant	**98.78**	96.65	97.70	418
Macro Avg	**98.18**	97.89	98.03	990

TABLE 10. Actual and predicted images by SVM classifier.

N=990	Predicted: Benign	Predicted: Malignant	
Actual Benign	TN=567	FP=5	572
Actual Malignant	FN=14	TP=404	418
	581	409	

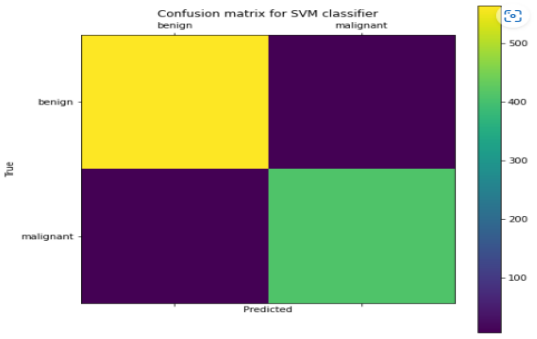

FIGURE 11. Confusion matrix using SVM Classifier.

F. DECISION TREE CLASSIFIER

The core nodes of the tree are utilized to represent the qualities to solve the problem, and each leaf node of the decision tree [53] corresponds to our class label, either benign or malignant. Any discrete attribute-based Boolean function can be represented using a decision tree. We were able to get an accuracy of 98.48% thanks to this classifier. Additionally, we looked into F1-score, recall, and precision. The classifier's results are as follows:

TABLE 11. Performance of decision tree classifier.

	Precision %	Recall %	F1-Score %	Support
Benign	**98.77**	98.60	98.69	572
Malignant	98.09	**98.33**	98.21	418
Macro Avg	98.43	**98.46**	98.45	990

TABLE 12. Actual and predicted images by DT classifier.

N=990	Predicted: Benign	Predicted: Malignant	
Actual Benign	TN=564	FP=8	572
Actual Malignant	FN=7	TP=411	418
	571	419	

G. RANDOM FOREST CLASSIFIER

From the features that were retrieved from our ISIC archive dataset, the random forest [54] selects a set of features at random. Afterward, a bootstrapped sample of the training data is used to create a classifier. Finally, unweighted voting is utilized to assign an unknown pixel to a class after trees (classifiers) are built. With the help of this classifier, we were able to achieve an accuracy of 99.46% using the ISIC 2017 dataset. We also considered the F1 score, recall, and precision. The following are the classification results:

TABLE 13. Performance of random forest classifier.

	Precision %	Recall %	F1-Score %	Support
Benign	**98.77**	98.60	98.69	572
Malignant	98.09	**98.33**	98.21	418
Macro Avg	98.43	**98.46**	98.45	990

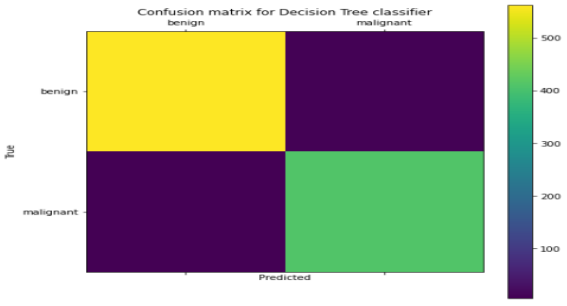

FIGURE 12. Confusion matrix using DT Classifier.

TABLE 14. Actual and predicted images by RF classifier.

N=990	Predicted: Benign	Predicted: Malignant	
Actual Benign	TN=563	FP=9	572
Actual Malignant	FN=6	TP=412	418
	569	421	

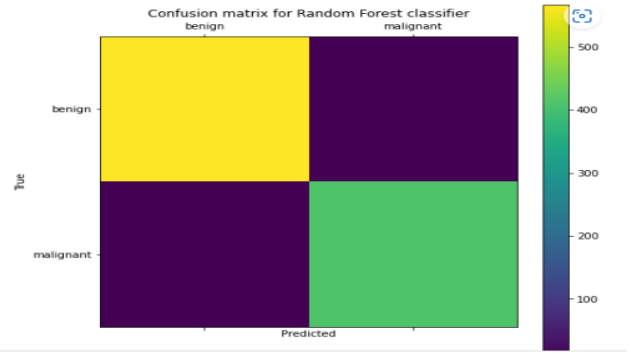

FIGURE 13. Confusion matrix using RF Classifier.

H. ROC CURVE

We used receiver operating characteristic (ROC) curves to comprehend the class reparability of the studied models, as given in figures 14, 15, and 16 for the ISIC 2017, ISIC 2019, and ISIC 2020 datasets, respectively. True positive rate (TPR) is charted against false positive rate (FPR) in an ROC curve by employing different thresh-olds at the probability results of the above classifiers. TPR assesses the probability of identifying malignant melanoma images. FPR, on the other hand, denotes the possibility of a false alarm in which a benign image is deemed to have melanoma symptoms. As shown in Figures 14 and 15, the ROC curve demonstrates the reliability of the proposed model, with the

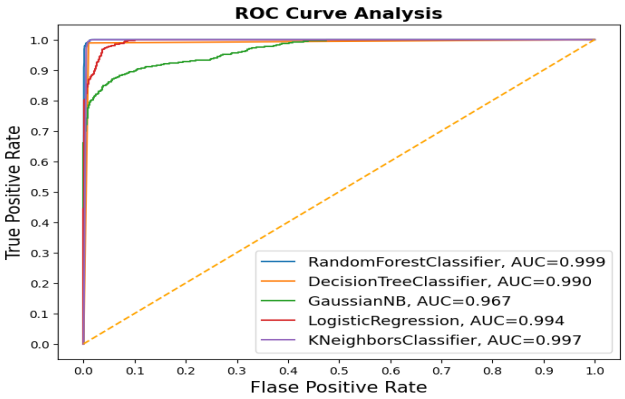

FIGURE 14. True and false positive rate of classifiers on ISIC 2017 dataset.

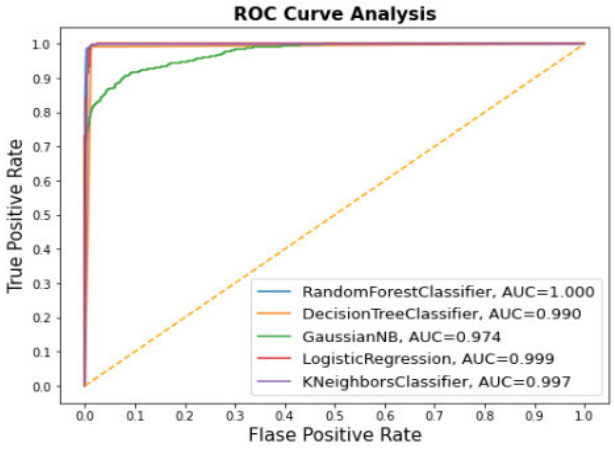

FIGURE 15. True and false positive rate of classifiers on ISIC 2019 dataset.

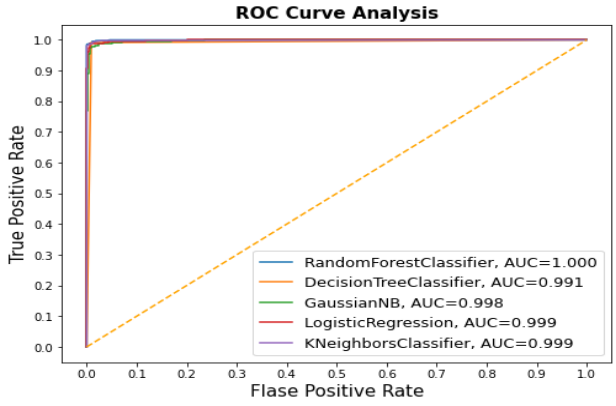

FIGURE 16. True and false positive rate of classifiers on ISIC 2020 dataset.

model attaining average AUC scores. In our study, the RF classifier significantly outperformed the other classifiers in terms of melanoma complication discrimination. Tables 3, 5, 7, 9, 11, and 13 demonstrate that the suggested model produces very few false positive (FP) and false negative (FN) cases. The lower the FP count, the lower the number of inaccurately identified positive encounters, and the higher the precision and specificity rates. In practice, keeping the number of FN cases low is also important because misidentifying a melanoma patient as healthy will seriously impede proper treatment. Based on the overall evaluation results, we conclude that the proposed model outperforms all other models studied.

V. CONCLUSION

In this study, we propose a novel approach on the basis of template matching for the accurate detection of ROI from image lesions. RGB dataset is transformed into gray scale to reduce computational requirements and improve visual image inspection. Features are extracted by the Haralick feature extractor and filtered through classifiers for comparative analysis. Experiments were applied on benchmark

datasets ISIC-2017, ISIC-2019, and ISIC-2020 archive, publicly available on the ISIC website. Our study outperformed the state-of-the-art algorithms and achieved the highest accuracy, Precision, Recall, and F1 Score of 99.46%, 99.65% (for Benign), 99.52% (for Malignant), and 99.39% respectively.

We also conducted a comparative study with state-of-the-art deep learning models and found our proposed work, normalized cross correlation-based k-means clustering model, outperformed deep learning models as shown above in Table 2.

Our study's prime focus was to detect melanoma as early as possible to avoid further complications. The proposed scheme successfully and accurately completed said task. The scheme is based on conventional techniques with low computational costs. The results achieved accuracy better than deep learning techniques. The study will be helpful to become a part of devices and apps for cancer detection.

STATEMENTS AND DECLARATIONS

COMPETING INTERESTS

There is no conflict of interest to declare.

AUTHORS' CONTRIBUTION STATEMENT

The authors of this paper, Muhammad Imran Faizi and Syed Muhammad Adnan, both contributed equally to the research and the writing of the paper. Specifically, both authors were involved in the conceptualization of the research, the design of the experiments, the data analysis, and the writing and revision of the paper.

ETHICAL AND INFORMED CONSENT FOR DATA USED

Ethical considerations: The ISIC-2017, ISIC-2019, and ISIC-2020 Dermoscopic Images used in this research project were obtained from the publicly available ISIC dataset, and no personal identifying information was collected or used. We followed appropriate ethical guidelines throughout the research process to ensure the privacy and confidentiality of the individuals whose images were included in the dataset.

As the images used in this research project were obtained from a publicly available dataset, we did not obtain individual informed consent from the individuals whose images are included. However, we ensured that appropriate ethical considerations were followed throughout the research process, and no personal identifying information was collected or used.

DATA AVAILABILITY AND ACCESS

The data used in this research project are publicly available and can be accessed through the International Skin Imaging Collaboration (ISIC) website (https://www.isic-archive.com/). The specific datasets used in this study are the ISIC-2017, ISIC-2019, and ISIC-2020 Dermoscopic Images are freely available to download.

REFERENCES

[1] M. Goyal, T. Knackstedt, S. Yan, and S. Hassanpour, "Artificial intelligence-based image classification methods for diagnosis of skin cancer: Challenges and opportunities," *Comput. Biol. Med.*, vol. 127, Dec. 2020, Art. no. 104065.

[2] N. Codella, V. Rotemberg, P. Tschandl, M. E. Celebi, S. Dusza, D. Gutman, B. Helba, A. Kalloo, K. Liopyris, M. Marchetti, H. Kittler, and A. Halpern, "Skin lesion analysis toward melanoma detection 2018: A challenge hosted by the international skin imaging collaboration (ISIC)," 2019, *arXiv:1902.03368*.

[3] J. Waring, C. Lindvall, and R. Umeton, "Automated machine learning: Review of the state-of-the-art and opportunities for healthcare," *Artif. Intell. Med.*, vol. 104, Apr. 2020, Art. no. 101822.

[4] A. Esteva, B. Kuprel, R. A. Novoa, J. Ko, S. M. Swetter, H. M. Blau, and S. Thrun, "Dermatologist-level classification of skin cancer with deep neural networks," *Nature*, vol. 542, no. 7639, pp. 115–118, Feb. 2017.

[5] Y. LeCun, Y. Bengio, and G. Hinton, "Deep learning," *Nature*, vol. 521, no. 7553, pp. 436–444, May 2015.

[6] T.-C. Pham, C.-M. Luong, M. Visani, and V.-D. Hoang, "Deep CNN and data augmentation for skin lesion classification," in *Intelligent Information and Database Systems*, vol. 10752, N. T. Nguyen, D. H. Hoang, T.-P. Hong, H. Pham, and B. Trawiński, Eds. Cham, Switzerland: Springer, 2018, pp. 573–582.

[7] J. Yap, W. Yolland, and P. Tschandl, "Multimodal skin lesion classification using deep learning," *Exp. Dermatol.*, vol. 27, no. 11, pp. 1261–1267, Nov. 2018.

[8] P. Tschandl et al., "Expert-level diagnosis of nonpigmented skin cancer by combined convolutional neural networks," *J. Amer. Med. Assoc. Dermatol.*, vol. 155, no. 1, p. 58, Jan. 2019.

[9] T. J. Brinker, A. Hekler, A. Hauschild, C. Berking, B. Schilling, A. H. Enk, S. Haferkamp, A. Karoglan, C. von Kalle, M. Weichenthal, E. Sattler, D. Schadendorf, M. R. Gaiser, J. Klode, and J. S. Utikal, "Comparing artificial intelligence algorithms to 157 German dermatologists: The melanoma classification benchmark," *Eur. J. Cancer*, vol. 111, pp. 30–37, Apr. 2019.

[10] J. Scharcanski and M. E. Celebi, *Computer Vision Techniques for the Diagnosis of Skin Cancer*. Berlin, Germany: Springer, 2014.

[11] M. E. Roberts and E. Claridge, "An artificially evolved vision system for segmenting skin lesion images," in *Medical Image Computing and Computer-Assisted Intervention—MICCAI*, vol. 2003, R. E. Ellis and T. M. Peters, Eds. Berlin, Germany: Springer, 2003, pp. 655–662.

[12] M. Silveira, J. C. Nascimento, J. S. Marques, A. R. S. Marçal, T. Mendonça, S. Yamauchi, J. Maeda, and J. Rozeira, "Comparison of segmentation methods for melanoma diagnosis in dermoscopy images," *IEEE J. Sel. Topics Signal Process.*, vol. 3, no. 1, pp. 35–45, Feb. 2009.

[13] A. Wong, J. Scharcanski, and P. Fieguth, "Automatic skin lesion segmentation via iterative stochastic region merging," *IEEE Trans. Inf. Technol. Biomed.*, vol. 15, no. 6, pp. 929–936, Nov. 2011.

[14] M. E. Yueksel and M. Borlu, "Accurate segmentation of dermoscopic images by image thresholding based on type-2 fuzzy logic," *IEEE Trans. Fuzzy Syst.*, vol. 17, no. 4, pp. 976–982, Aug. 2009.

[15] H. Zhou, G. Schaefer, M. E. Celebi, H. Iyatomi, K.-A. Norton, T. Liu, and F. Lin, "Skin lesion segmentation using an improved snake model," in *Proc. Annu. Int. Conf. IEEE Eng. Med. Biol.*, Aug. 2010, pp. 1974–1977.

[16] Q. Abbas, I. Fondón, and M. Rashid, "Unsupervised skin lesions border detection via two-dimensional image analysis," *Comput. Methods Programs Biomed.*, vol. 104, no. 3, pp. e1–e15, Dec. 2011.

[17] C. A. Z. Barcelos and V. B. Pires, "An automatic based nonlinear diffusion equations scheme for skin lesion segmentation," *Appl. Math. Comput.*, vol. 215, no. 1, pp. 251–261, Sep. 2009.

[18] F. Kaleli, N. Aydin, G. Ertas, and H. O. Gulcur, "An adaptive approach to the segmentation of DCE-MR images of the breast: Comparison with classical thresholding algorithms," in *Proc. IEEE Symp. Comput. Intell. Image Signal Process.*, Apr. 2007, pp. 375–379.

[19] H. U. Rehman, N. Nida, S. A. Shah, W. Ahmad, M. I. Faizi, and S. M. Anwar, "Automatic melanoma detection and segmentation in dermoscopy images using deep RetinaNet and conditional random fields," *Multimedia Tools Appl.*, vol. 81, no. 18, pp. 25765–25785, Jul. 2022.

[20] T. Saba, "Computer vision for microscopic skin cancer diagnosis using handcrafted and non-handcrafted features," *Microsc. Res. Technique*, vol. 84, no. 6, pp. 1272–1283, Jun. 2021.

[21] W. Rizwan, S. M. Adnan, W. Ahmed, and M. I. Faizi, "Skin lesions detection and classification using deep learning," *Warse*, vol. 10, no. 3, pp. 1720–1728, Jun. 2021.

[22] H. Alquran, I. A. Qasmieh, A. M. Alqudah, S. Alhammouri, E. Alawneh, A. Abughazaleh, and F. Hasayen, "The melanoma skin cancer detection and classification using support vector machine," in *Proc. IEEE Jordan Conf. Appl. Electr. Eng. Comput. Technol. (AEECT)*, Oct. 2017, pp. 1–5.

[23] C. A. Ferreira, A. Cunha, A. M. Mendonça, and A. Campilho, "Convolutional neural network architectures for texture classification of pulmonary nodules," in *Progress in Pattern Recognition, Image Analysis, Computer Vision, and Applications*, vol. 11401, R. Vera-rodriguez, J. Fierrez, and A. Morales, Eds. Cham, Switzerland: Springer, 2019, pp. 783–791.

[24] A.-R. Ali, J. Li, G. Yang, and S. J. O'Shea, "A machine learning approach to automatic detection of irregularity in skin lesion border using dermoscopic images," *PeerJ Comput. Sci.*, vol. 6, p. e268, Jun. 2020.

[25] A.-R. Ali, J. Li, and S. J. O'Shea, "Towards the automatic detection of skin lesion shape asymmetry, color variegation and diameter in dermoscopic images," *PLoS One*, vol. 15, no. 6, Jun. 2020, Art. no. e0234352.

[26] J. R. Hagerty, R. J. Stanley, H. A. Almubarak, N. Lama, R. Kasmi, P. Guo, R. J. Drugge, H. S. Rabinovitz, M. Oliviero, and W. V. Stoecker, "Deep learning and handcrafted method fusion: Higher diagnostic accuracy for melanoma dermoscopy images," *IEEE J. Biomed. Health Inform.*, vol. 23, no. 4, pp. 1385–1391, Jul. 2019.

[27] P. M. M. Pereira, R. Fonseca-Pinto, R. P. Paiva, P. A. A. Assuncao, L. M. N. Tavora, L. A. Thomaz, and S. M. M. Faria, "Dermoscopic skin lesion image segmentation based on local binary pattern clustering: Comparative study," *Biomed. Signal Process. Control*, vol. 59, May 2020, Art. no. 101924.

[28] R. Das, S. De, S. Bhattacharyya, J. Platos, V. Snasel, and A. E. Hassanien, "Data augmentation and feature fusion for melanoma detection with content based image classification," in *Proc. Int. Conf. Adv. Mach. Learn. Technol. Appl.*, vol. 921, A. E. Hassanien, A. T. Azar, T. Gaber, R. Bhatnagar, and M. F. Tolba, Eds. Cham, Switzerland: Springer, 2020, pp. 712–721.

[29] A. Rehman, M. A. Khan, Z. Mehmood, T. Saba, M. Sardaraz, and M. Rashid, "Microscopic melanoma detection and classification: A framework of pixel-based fusion and multilevel features reduction," *Microsc. Res. Technique*, vol. 83, no. 4, pp. 410–423, Apr. 2020.

[30] Y. Li and L. Shen, "Skin lesion analysis towards melanoma detection using deep learning network," *Sensors*, vol. 18, no. 2, p. 556, Feb. 2018.

[31] N. C. F. Codella, Q.-B. Nguyen, S. Pankanti, D. A. Gutman, B. Helba, A. C. Halpern, and J. R. Smith, "Deep learning ensembles for melanoma recognition in dermoscopy images," *IBM J. Res. Develop.*, vol. 61, nos. 4–5, pp. 1–15, Jul. 2017.

[32] O. Abuzaghleh, B. D. Barkana, and M. Faezipour, "Noninvasive real-time automated skin lesion analysis system for melanoma early detection and prevention," *IEEE J. Transl. Eng. Health Med.*, vol. 3, pp. 1–12, 2015.

[33] C. Barata, M. Ruela, M. Francisco, T. Mendonça, and J. S. Marques, "Two systems for the detection of melanomas in dermoscopy images using texture and color features," *IEEE Syst. J.*, vol. 8, no. 3, pp. 965–979, Sep. 2014.

[34] G. Capdehourat, A. Corez, A. Bazzano, R. Alonso, and P. Musé, "Toward a combined tool to assist dermatologists in melanoma detection from dermoscopic images of pigmented skin lesions," *Pattern Recognit. Lett.*, vol. 32, no. 16, pp. 2187–2196, Dec. 2011.

[35] P. Rubegni, G. Cevenini, M. Burroni, R. Perotti, G. Dell'Eva, P. Sbano, C. Miracco, P. Luzi, P. Tosi, P. Barbini, and L. Andreassi, "Automated diagnosis of pigmented skin lesions," *Int. J. Cancer*, vol. 101, no. 6, pp. 576–580, Oct. 2002.

[36] H. Ganster, P. Pinz, R. Rohrer, E. Wildling, M. Binder, and H. Kittler, "Automated melanoma recognition," *IEEE Trans. Med. Imag.*, vol. 20, no. 3, pp. 233–239, Mar. 2001.

[37] A. Gupta, S. Thakur, and A. Rana, "Study of melanoma detection and classification techniques," in *Proc. 8th Int. Conf. Rel., INFOCOM Technol. Optim. (ICRITO)*, Jun. 2020, pp. 1345–1350.

[38] R. Brunelli, *Template Matching Techniques in Computer Vision: Theory and Practice*. Chichester, U.K.: Wiley, 2009, pp. 1–7.

[39] L. Cole, D. Austin, and L. Cole, "Visual object recognition using template matching," in *Proc. Austral. Conf. Robot. Automat.*, Dec. 2004, pp. 10–17. [Online]. Available: https://www.araa.asn.au/acra/acra2004/papers/cole.pdf

[40] A. M. Society, "Mathematical reviews," Amer. Math. Soc., Austral. Nat. Univ., Providence, RI, USA, Tech. Rep., 2004.

[41] M. F. J. Acosta, L. Y. C. Tovar, M. B. Garcia-Zapirain, and W. S. Percybrooks, "Melanoma diagnosis using deep learning techniques on dermatoscopic images," *BMC Med. Imag.*, vol. 21, no. 1, Dec. 2021.

[42] I. A. Alfi, M. M. Rahman, M. Shorfuzzaman, and A. Nazir, "A non-invasive interpretable diagnosis of melanoma skin cancer using deep learning and ensemble stacking of machine learning models," *Diagnostics*, vol. 12, no. 3, p. 726, Mar. 2022.

[43] Y. Wan, Y. Cheng, and M. Shao, "MSLANet: Multi-scale long attention network for skin lesion classification," *Int. J. Speech Technol.*, vol. 53, no. 10, pp. 12580–12598, May 2023.

[44] S. M. Jaisakthi, M. P, C. Aravindan, and R. Appavu, "Classification of skin cancer from dermoscopic images using deep neural network architectures," *Multimedia Tools Appl.*, vol. 82, no. 10, pp. 15763–15778, Apr. 2023.

[45] S. Qasim Gilani, T. Syed, M. Umair, and O. Marques, "Skin cancer classification using deep spiking neural network," *J. Digit. Imag.*, vol. 36, no. 3, pp. 1137–1147, Jan. 2023.

[46] M.-K. Hu, "Visual pattern recognition by moment invariants," *IEEE Trans. Inf. Theory*, vol. IT-8, no. 2, pp. 179–187, Feb. 1962.

[47] R. J. Prokop and A. P. Reeves, "A survey of moment-based techniques for unoccluded object representation and recognition," *Graph. Models Image Process.*, vol. 54, no. 5, pp. 438–460, Sep. 1992.

[48] R. M. Haralick, K. Shanmugam, and I. Dinstein, "Textural features for image classification," *IEEE Trans. Syst., Man, Cybern.*, vol. SMC-3, no. 6, pp. 610–621, Nov. 1973.

[49] D. Srivastava, R. Bakthula, and S. Agarwal, "Image classification using SURF and bag of LBP features constructed by clustering with fixed centers," *Multimedia Tools Appl.*, vol. 78, no. 11, pp. 14129–14153, Jun. 2019.

[50] Q. Tian, L. F. Yan, X. Zhang, X. Zhang, Y. C. Hu, Y. Han, Z. C. Liu, H. Y. Nan, Q. Sun, Y. Z. Sun, Y. Yang, Y. Yu, J. Zhang, B. Hu, and G. B. Cui, "Radiomics strategy for glioma grading using texture features from multiparametric MRI," *J. Magn. Reson. Imag.*, vol. 48, no. 6, pp. 1518–1528, Dec. 2018.

[51] X. Ou, W. Pan, and P. Xiao, "In vivo skin capacitive imaging analysis by using grey level co-occurrence matrix (GLCM)," *Int. J. Pharmaceutics*, vol. 460, nos. 1–2, pp. 28–32, Jan. 2014.

[52] Y. Liao and V. R. Vemuri, "Use of K-nearest neighbor classifier for intrusion detection," *Comput. Secur.*, vol. 21, no. 5, pp. 439–448, Oct. 2002.

[53] A. Widodo and B.-S. Yang, "Support vector machine in machine condition monitoring and fault diagnosis," *Mech. Syst. Signal Process.*, vol. 21, no. 6, pp. 2560–2574, Aug. 2007.

[54] P. Mishra, D. Singh, and Y. Yamaguchi, "Land cover classification of PALSAR images by knowledge based decision tree classifier and supervised classifiers based on SAR observables," *Prog. Electromagn. Res. B*, vol. 30, pp. 47–70, 2011.

[55] M. Pal, "Random forest classifier for remote sensing classification," *Int. J. Remote Sens.*, vol. 26, no. 1, pp. 217–222, Jan. 2005.

[56] Kaggle. (2019). *ISIC 2019 Dataset*. Accessed: Sep. 10, 2022. [Online]. Available: https://www.kaggle.com/fanconic/skin-cancer-malignant-vs-benign

[57] L. Breiman, "Random forests," *Mach. Learn.*, vol. 45, pp. 5–32, Oct. 2001.

[58] J. R. Quinlan, "Induction of decision trees," *Mach. Learn.*, vol. 1, no. 1, pp. 81–106, Mar. 1986.

[59] C. Cortes and V. Vapnik, "Support-vector networks," *Mach. Learn.*, vol. 20, no. 3, pp. 273–297, Sep. 1995.

[60] I. H. Witten, E. Frank, M. A. Hall, and C. J. Pal, *Data Mining: Practical Machine Learning Tools and Techniques*, 2nd ed. San Francisco, CA, USA: Morgan Kaufmann, 2005, p. 121.

[61] D. R. Cox, "The regression analysis of binary sequences," *J. Roy. Stat. Soc., B, Methodol.*, vol. 34, pp. 187–220, 1972.

[62] T. Cover and P. Hart, "Nearest neighbor pattern classification," *IEEE Trans. Inf. Theory*, vol. IT-13, no. 1, pp. 21–27, Jan. 1967.

[63] R. Rout, P. Parida, and D. Sonali, "Automatic skin lesion segmentation using a hybrid deep learning network," *Int. J. Comput. Inf. Syst. Ind. Manag. Appl.*, vol. 15, pp. 238–249, 2150.

[64] S. Dash, P. Parida, and J. R. Mohanty, "Illumination robust deep convolutional neural network for medical image classification," *Soft Comput.*, Feb. 2023.

[65] R. Rout, P. Parida, Y. Alotaibi, S. Alghamdi, and O. I. Khalaf, "Skin lesion extraction using multiscale morphological local variance reconstruction based watershed transform and fast fuzzy c-means clustering," *Symmetry*, vol. 13, no. 11, p. 2085, Nov. 2021.

[66] R. Rout and P. Parida, "A novel method for melanocytic skin lesion extraction and analysis," *J. Discrete Math. Sci. Cryptogr.*, vol. 23, no. 2, pp. 461–473, Feb. 2020.
[67] R. Rout, P. Priyadarsan, and D. Sonali, "A hybrid deep learning network for skin lesion extraction," in *Proc. Int. Conf. Soft Comput. Pattern Recognit.*, 2023, pp. 682–689 doi: 10.1007/978-3-031-27524-1_66.
[68] R. Rout, P. Parida, and S. Patnaik, "Melanocytic skin lesion extraction using mean shift clustering," in *Proc. Int. Conf. Electron. Inf. Technol. Smart Agricult. (ICEITSA)*, Huaihua, China, Dec. 2021, pp. 565–574.

MUHAMMAD IMRAN FAIZI received the M.S. degree in computer science from the University of South Asia, Lahore, Punjab, Pakistan, in 2015. He is currently pursuing the Ph.D. degree with the Department of Computer Science, University of Engineering and Technology Taxila, Punjab. He has been with the University of Chakwal, Punjab, as a Visiting Faculty Member, since 2020. He has 15 years of teaching and administration and three years of research experience. His research interests include computer vision, image processing, artificial intelligence, and machine learning.

SYED MUHAMMAD ADNAN received the M.S. degree in computer engineering from the Center for Advanced Studies in Engineering (CASE), Islamabad, Pakistan, in 2010, and the Ph.D. degree in computer engineering from the University of Engineering and Technology Taxila, Pakistan, in 2014. Currently, he is an Assistant Professor with the Department of Computer Science, University of Engineering and Technology Taxila. His research interests include acoustic scene analysis, computer vision, multimedia signal processing, and machine learning.